Experimental Mechanics (2017) 57:637–648
DOI 10.1007/s11340-017-0257-3

Inverse Estimation of Cohesive Fracture Properties of Asphalt Mixtures Using an Optimization Approach

B.C. Hill[1] · **O. Giraldo-Londoño**[2] · **G.H. Paulino**[2] · **W.G. Buttlar**[3]

Received: 4 February 2016 / Accepted: 25 January 2017 / Published online: 14 February 2017

Abstract Tensile cracking in asphalt pavements due to vehicular and thermal loads has become an experimental and numerical research focus in the asphalt materials community. Previous studies have used the discrete element method (DEM) to study asphalt concrete fracture. These studies used trial-and-error to obtain local fracture properties such that the DEM models approximate the experimental load-crack mouth opening displacement response. In the current study, we identify the cohesive fracture properties of asphalt mixtures via a nonlinear optimization method. The method encompasses a comparative investigation of displacement fields obtained using both digital image correlation (DIC) and heterogeneous DEM fracture simulations. The proposed method is applied to two standard fracture test geometries: the single-edge notched beam test, SE(B), under three-point bending, and the disk-shaped compact tension test, DC(T). For each test, the Subset Splitting DIC algorithm is used to determine the displacement field in a predefined region near the notch tip. Then, a given number of DEM simulations are performed on the same specimen. The DEM is used to simulate the fracture of asphalt concrete with a linear softening cohesive contact model, where fracture-related properties (e.g., maximum tensile force and maximum crack opening) are varied within a predefined range. The difference between DIC and DEM displacement fields for each set of fracture parameters is then computed and converted to a continuous function via multivariate Lagrange interpolation. Finally, we use a Newton-like optimization technique to minimize Lagrange multinomials, yielding a set of fracture parameters that minimizes the difference between the DEM and DIC displacement fields. The optimized set of fracture parameters from this nonlinear optimization procedure led to DEM results which are consistent with the experimental results for both SE(B) and DC(T) geometries.

Keywords DEM · DIC · Asphalt · Fracture · DC(T) · Optimization

✉ W. G. Buttlar
buttlarw@missouri.edu

[1] Department of Civil and Environmental Engineering, University of Illinois, Urbana, IL 61801, USA

[2] School of Civil and Environmental Engineering, Georgia Institute of Technology, Atlanta, GA 30332, USA

[3] Department of Civil and Environmental Engineering, University of Missouri, Columbia, MO 65211, USA

Introduction

Asphalt pavement roughness, generated by cracks developed via vehicular and thermal loads, has led to significant increases in user cost [1]. Due to weakness in tension of cementitious materials such as asphalt, cracks generally form in a tensile fashion. This has led the paving industry to invest in academic research studies aimed at developing fracture test geometries as well as numerical modeling applications to identify local material fracture properties. Local asphalt fracture properties have been employed to compare trial mixtures containing new materials to a quality performing reference mixture or to model full-scale pavement sections. Previous research involving beam and disk-shaped compact tension fracture geometries of asphalt mixtures has achieved experimental repeatability in global material response and correlation with field performance [2, 3]. Presently, considerable emphasis is being placed on coupling numerical simulations with asphalt fracture experiments, in order to identify local fracture properties via matching the results at the global and local

scales. We believe that coupling numerical and experimental results at the local scale, e.g., by matching the displacement field during a fracture test, will help to advance our understanding of asphalt mixture fracture.

The discrete element method (DEM) is a numerical modeling tool that is highly applicable to the modeling of fracture in heterogeneous materials such as hot mix asphalt (HMA) [4–9]. Hot mix asphalt can be assumed to be composed of aggregates, mastic, and interfaces between aggregates and mastic [9]. A typical fracture analysis of HMA in the context of DEM requires input parameters defining bulk material behavior as well as fracture-related properties. These properties allow for the definition of the interaction between the particles used to simulate the fracture.

The determination of local fracture properties such as fracture energy and cohesive strength through numerical simulations is a nontrivial task. For example, if the fracture properties obtained experimentally are directly used to perform heterogeneous DEM simulations, the numerical output obtained often differs from the actual behavior of the tested specimen. As a result, calibration of these properties is needed to determine representative parameters for simulations [4]. Previous researchers have performed this calibration by visually comparing the global response of the specimen with the results of heterogeneous DEM simulations (e.g., calibration based of load vs. crack mouth opening displacement (CMOD) curves) [4, 8, 9]. This approach, however, does not guarantee that the simulation will accurately predict the local behavior of the tested specimen. In other words, simulated results based on parameters calibrated from global load-CMOD curves may yield inaccurate prediction of the full crack profile, and therefore, may not accurately capture the local fracture behavior.

Calibrated fracture parameters can be obtained through single or full displacement field experimental measurements. For instance, Aragão and Kim [10], Kim and Aragão [11], and Im et al. [12] used digital image correlation (DIC) to measure CMOD values in a fine aggregate matrix to identify local fracture parameters which match FEM simulations. However, notice that their calibration is based on a global quantity (i.e., the CMOD), and not on full displacement fields. Local fracture properties obtained from multiple displacement field measurements on the specimen surface, and ahead of the crack tip, can help to improve the prediction of material response obtained from simulations. Consequently, we have used the local displacement fields found through the DIC rather than the CMOD measurement alone. Some studies have used full displacement fields to obtain the fracture parameters of different materials. Pop et al. [13] used full displacement field experimental measurements to characterize FEM fracture parameters for isotropic media. In that study, the FE models were elastic and isotropic, and no crack propagation was considered. In addition, Shen and Paulino [14, 15] used a hybrid inverse technique to estimate the cohesive fracture properties of a ductile adhesive and a quasi-brittle plastic [14], and fiber-reinforced cementitious composites [15], by comparing the DIC measurements of the displacement fields with the results of FEM simulations. To simulate crack propagation, Shen and Paulino [14, 15] used the so-called cohesive zone model (CZM) approach. In their studies, the CZM was constructed by means of a spline curve passing through a series of control points that were determined using the Nelder-Mead optimization method. This is a derivative-free method to determine the cohesive fracture parameters, which requires hundreds of iterations to converge. The main limitations of those investigations are: 1) the crack path in the FEM simulations was predefined to be a straight line; and 2) the FEM models were elastic and homogeneous, neglecting time dependency, i.e., viscoelastic effects.

The main goal of the current study is to use DIC and DEM displacement field measurements to obtain the local fracture properties for heterogeneous asphalt mixtures. This methodology can be used by academicians and higher level mixture design firms to optimally design asphalt mixtures in terms of low-temperature fracture resistance. In contrast to previous coupled experimental and numerical studies, no predefined crack path is chosen. A nonlinear optimization method for obtaining the cohesive fracture properties of asphalt mixtures is proposed in the current study. The method aims to minimize the difference between measured (DIC) and simulated (DEM) displacement fields, using a set of DEM fracture simulations. To achieve this, the measure of the difference between DEM and DIC displacement fields for a predefined set of fracture parameters is used to construct a continuous function based on multivariate Lagrange interpolation. This function is then used to minimize the difference between measured and simulated displacement fields using Newton-like optimization methods. The DEM simulations are performed using the software PFC-2D - see Cundall and Strack [16]. In the DEM simulations, fracture is modeled using linear softening cohesive contacts. The optimized set of fracture parameters obtained from the nonlinear optimization procedure led to DEM results that were in good agreement with experimental results found using both SE(B) and DC(T) geometries.

Experimental Procedure

The experimental portion of the study evaluates an aggregate-asphalt surface mixture with original materials (no recycled material content, additives, or modifiers). The mixture is a PG 64–22 9.5 mm nominal maximum aggregate size mixture containing dolomitic limestone aggregate. Cylindrical specimens are created in the laboratory following the Superpave asphalt mixture design specifications [17]. The cylinders are compacted such that they contain approximately 7.0 ± 0.5% air voids, following the ASTM D7313–13 volumetric

protocols [18]. Both asphalt concrete beam, SE(B), and disk-shaped compact tension test, DC(T), geometries are used in the current study to evaluate fracture resistance of asphalt mixtures. Fracture resistance is determined by characterizing the pre- and post-peak Load-CMOD behavior. The primary testing result is a measure of fracture energy, which is obtained by determining the area under the load-CMOD plot, which is normalized by the fractured specimen area. An example plot of load-CMOD curves, in this case for SE(B) specimens, is shown in Fig. 1 with a test temperature of -12 °C. The DC(T) test is conducted in accordance with the ASTM D7313-13 [18]. The test is conducted using an Instron 8500 servo-hydraulic system in CMOD displacement control at an opening rate of 1.0 mm/min. A conditioning chamber surrounds the testing set-up in order to maintain a constant test temperature, which in this case, was set at −12 °C.

The beam test geometry, SE(B), and loading rate are chosen in this study based on earlier experimental observations of Wagoner et al. [2]. The SE(B) specimens are cut from Superpave gyratory cylinders using masonry and tile saws. Specimens are initially sliced to a 40 mm thickness with 2 cuts using a masonry saw. A tile saw is used to slice the ends of the specimens to reach the span length shown in Fig. 2. The same tile saw is also used to insert the notch. The geometry shown in Fig. 2 has a thickness of 40 mm and has a ligament of 45 mm, which is shorter than the one in DC(T) geometry. However, a consistent value of 0.25 for the notch to depth (a/W) ratio remains the same in both cases. This ratio was maintained at 0.25 to increase the remaining ligament length and reduce variability caused by the heterogeneous nature of the asphalt mixture. It should be noted that the beam dimensions differ from those of Wagoner et al. [2]. A smaller beam specimen, as shown in Fig. 2, is considered in this study due to the small nominal maximum aggregate size (NMAS) of the asphalt mixture. The loading rate is chosen as 0.5 mm/min such that the peak load occurs approximately five seconds after reaching the asphalt concrete strength criteria discussed by Wagoner et al. [2]. The same environmental cooling chamber, data acquisition system, and servo-hydraulic machine as the DC(T) test are used to avoid additional study variables.

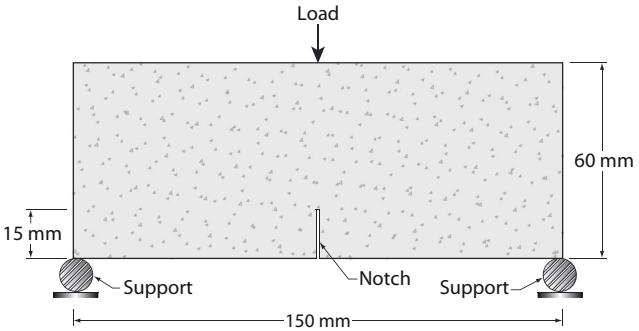

Fig. 2 Asphalt concrete beam 'SE(B)' geometry

The DEM particle stiffness properties are determined using the indirect tension (IDT) test. Both mastic (asphalt cement and aggregate smaller than 2.36 mm) and the full 9.50 mm NMAS mixture are tested according to the AASHTO T-322 IDT creep compliance test method [19]. Mastic and mixture creep compliance test results are shown in Fig. 3. It should be noted that the mastic creep compliance is higher than the mixture due to the lack of coarser aggregates. The mastic creep compliance results, later converted to relaxation modulus, are used for the remainder of the study as the mastic stiffness properties in the heterogeneous DEM simulations. The mastic particle size limit is chosen to coincide with the definition provided by Kim et al. [8]. The IDT testing is accomplished at −12 °C for a period of 1000 s to capture the time dependent material response. The experimental creep compliance was fitted using the Burger's model as shown in equation (1):

$$D(\xi) = D_1 + \frac{\xi}{\eta_1} + D_2\left(1 - e^{-\xi/\tau_2}\right) \tag{1}$$

where ξ is reduced time, $D(\xi)$ is the creep compliance at the reduced time ξ, and D_i, τ_i, and η_i are fitted model constants.

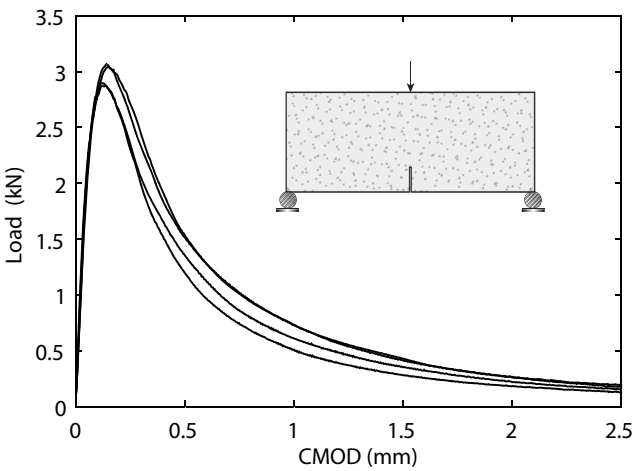

Fig. 1 Example load-CMOD results (four replicates of the same mixture)

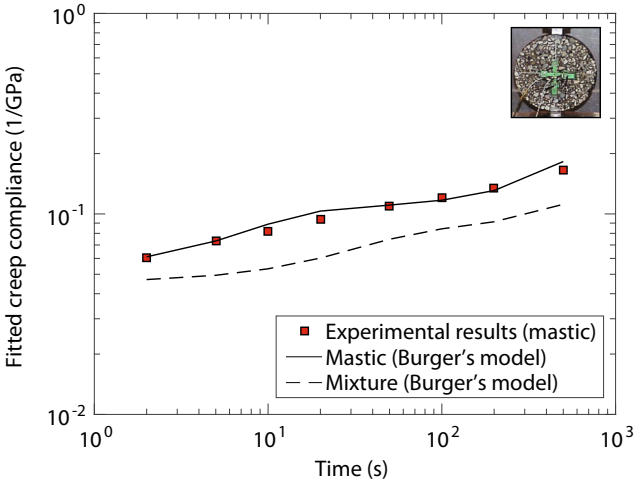

Fig. 3 Creep compliance test results for a temperature $T = -12$ °C

The Prony Series model is the most widely used phenomenological model in asphalt concrete creep compliance research. However, to perform the DEM simulations, we used the PFC2D 4.0 version software, which only has Burger's model functionality. It should be noted that the built-in Burger's model contact in PFC2D 4.0 does not allow cohesive softening. Consequently, this study modifies the built-in model contact to allow for cohesive softening as discussed below in the "Discrete Element Modeling" section. As shown in Fig. 3, the Burger's model fits the experimental data well for the materials and test temperature used in this study. In order to evaluate the relaxation modulus of the mastic, interconversion, as discussed in Park and Kim [20], is used.

DIC Approach

In this study, DIC is used to evaluate the displacement fields found in both SE(B) and DC(T) fracture tests. In the past, researchers developed DIC matching algorithms, such as the subset DIC method, to determine displacement and resulting strain fields [21–24]. A full-field matching algorithm, employed by Shen and Paulino [14] in the area of cementitious materials, yielded improved DIC correlation performance in comparison to the traditional subset DIC method. However, the DIC matching method used by Shen and Paulino [14] is not directly applicable in this study due to unpredictability of the crack path in heterogeneous material fracture. Thus, we use the Subset Splitting method by Poissant and Barthelat [25], to evaluate DIC displacement fields, due to its ability to consider heterogeneous crack growth. Linear shape functions are used in this study in conjunction with the Subset Splitting method. The linear shape functions are shown below in equation (2):

$$u(i,j) = u + \frac{\partial u}{\partial x} i + \frac{\partial u}{\partial y} j \text{ , and } v(i,j) = v + \frac{\partial v}{\partial x} i + \frac{\partial v}{\partial y} j \tag{2}$$

where u and v are the horizontal displacement and vertical displacement of the subset. The best match of linear shape function parameters, $q = \left(u, v, \frac{\partial u}{\partial x}, \frac{\partial u}{\partial y}, \frac{\partial v}{\partial x}, \frac{\partial v}{\partial y}\right)$, yields the lowest cumulative difference in pixel intensities found using a least-squares matching correlation coefficient. Poissant and Barthelat [25] determined that subsets could be split into master and slave subsets containing a discontinuity such that optimized parameters sets, q_{master} and q_{slave}, were determined via a Newton-Raphson approach.

In order to use the Subset Splitting method [25], the asphalt samples are photographed during the fracture tests at a predefined image capture rate. Images are taken using a 2MP Stingray F-201C CCD camera and a Tamron 50 mm lens at a range of 1.0 m from the specimen. All images are taken perpendicular to the specimen surface as shown in Fig. 4. Imaging at a distance of approximately 1.0 m is possible due to the glass viewport of the cooling chamber. The viewport is larger than the test specimens to allow imaging throughout the test without opening the chamber and subjecting warm air to the specimens. During testing, all the ceiling lights in the laboratory were turned off to avoid interference with the LED lights of the DIC system. The images are taken at a rate of 5 frames per second and are cropped to 1300 pixels by 1000 pixels for the SE(B) and 1300 pixels by 1200 pixels for the DC(T) specimens. The images are cropped to remove the presence of the notch in the analyzed images. The remaining image region is named the region of interest (ROI). The ROI, for both DC(T) and SE(B) geometries, in this case, is approximately 45 mm length by 45 mm in height, as depicted in Fig. 5a and b. The data collection of load and CMOD measurements from the experiment and DIC images are synced manually. This syncing process is completed by first identifying the imaging rate of the camera and Load-CMOD data acquisition rate. Then, the image of initial load application is found by manually parsing through images until movement is found. As a result, with the previously found rates and initial loading image, the images and load-CMOD data are synchronized. Table 1 shows the DIC parameters describing the camera, imaging distance, and resolution in the present study.

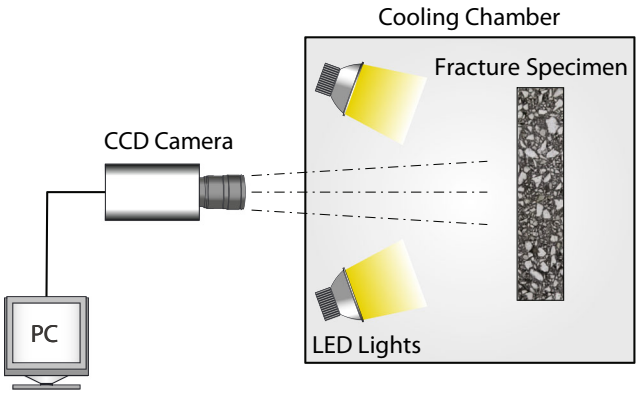

Fig. 4 Schematic of the set-up used to collect the images used in the DIC algorithm. A Stingray F-201C camera located 1 m from the specimens is used to obtain the images during the fracture tests for both SE(B) and DC(T) geometries. (Adapted from Hill and Buttlar [26])

Discrete Element Modeling

In the literature, You and Buttlar [27] used the DEM approach to obtain asphalt mixture complex modulus response for various temperatures and load frequencies. In addition, Kim et al. [6–8] successfully used the DEM approach to model fracture in homogeneous and heterogeneous asphalt mixtures. In this study, we use the DEM approach to simulate crack propagation for both SE(B) and DC(T) geometries. Each geometry is discretized using rigid circular elements, and the simulations

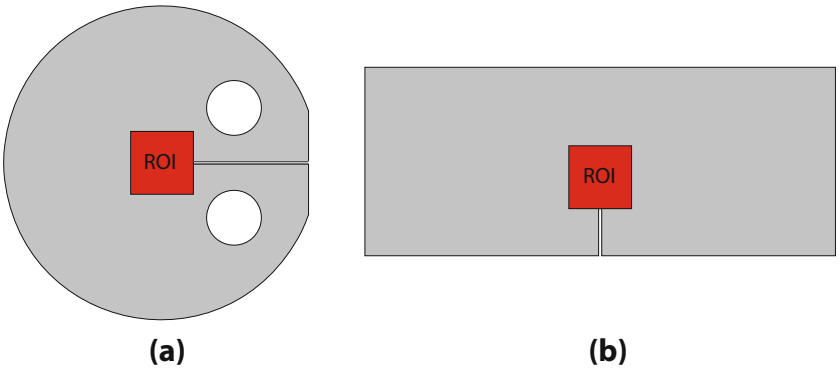

Fig. 5 Regions of interest (ROI) of 45 mm by 45 mm used to measure the DIC displacement fields during the fracture tests for: (**a**) DC(T) geometry; and (**b**) SE(B) geometry

are performed using the particle flow code in two dimensions, PFC-2D [16]. Notice that the present study is focused on 2D heterogeneous fracture simulations; however, the fracture tests are actually in three dimensions. In order to model an actual three-dimensional fracture test using a two-dimensional computational model, some general issues related to heterogeneous modeling of asphalt mixtures need to be accounted for. The DIC system, illustrated by Fig. 4, only allows measurements of 2D surface deformations in the horizontal and vertical (planar) directions. Other experimental techniques could be investigated to measure displacement fields and thus the reader is referred to the appropriate references [28–30]. Here 2D (planar) DIC fields measured from the 3D fracture test and 2D DEM modeling are used to couple the experiments with the simulations. Previous studies by Shen and Paulino [14, 15] in adhesives and cementitious materials have used the approach of planar DIC and 2D FEM simulations to determine the applicability of a nonlinear optimization method. Consequently, the use of 2D plane strain DEM simulations is chosen in this study to evaluate the applicability of this optimization method.[1]

The DEM equilibrium equation is provided below in equation (3) in addition to the force increment equation:

$$\mathbf{Ma} + \mathbf{K}\Delta\mathbf{x} = \Delta\mathbf{f} \quad , \quad \Delta\mathbf{f} = \mathbf{K}\Delta\mathbf{u} \tag{3}$$

where **M** is the mass of the particle, **a** is the acceleration of the particle, **K** is the stiffness matrix, $\Delta\mathbf{x}$ ($\Delta\mathbf{u}$) is the incremental displacement, and $\Delta\mathbf{f}$ is the incremental force. Before damage has occurred, the stiffness matrix **K** is constructed based on linear contact models between adjacent particles in the DEM "mesh" [8]. The linear contacts are defined in terms of the normal and shear contact stiffness between particles, K^n and K^s, respectively. The contact stiffness depends on the particle packing arrangement. In the study by Kim et al. [8], different particle packing arrangements were discussed, including square, hexagonal, and random. It is known that a square particle packing in DEM cannot generate a Poisson's effect. To circumvent this problem, a hexagonal packing arrangement is used. A hexagonal particle packing offers both the possibility to simulate Poisson's effect and assign contact properties in a straightforward way. Kim et al. [8] presented expressions for the normal and shear contact stiffness between adjacent particles, K^n and K^s, by equating the strain energy of the DEM-based model and that from a two-dimensional plane strain continuum model, leading to:

$$K^n = \frac{E}{\sqrt{3}(1+\nu)(1-2\nu)} \quad \text{, and} \quad K^s = \frac{E(1-4\nu)}{\sqrt{3}(1+\nu)(1-2\nu)} \tag{4}$$

where E is the elastic modulus and ν is the Poisson's ratio. Note that the contact stiffness shown in equation (4) are developed for a hexagonal particle packing arrangement [8]. In order to model damage development in asphalt during fracture processes, all particle bonds utilize linear softening cohesive contacts. An example of the linear softening cohesive law is provided below in Fig. 6 and a complete description of the DEM implementation of linear cohesive softening is provided in Kim et al. [8]. An additional user-defined viscoelastic cohesive contact is employed in this study to consider the time-dependent response of the mastic. Asphalt mastic and thus

Table 1 DIC Imaging Parameters

DIC Technique	Subset Splitting
Sensor/Digitization	1624p x 1234p/8-bit
Lens Mount	C Mount
Image Capture Rate	5 Hz
Scaling	0.0439 mm/pixel
Subset/Step Size	25/6
Interpolation Method	Bicubic B-spline
Correlation Criteria	< 0.004
Image Pre-processing	LUT Brightness Adjustment
Displacement Resolution	0.004p

[1] Future research could explore 3D DEM simulations using DIC measurements.

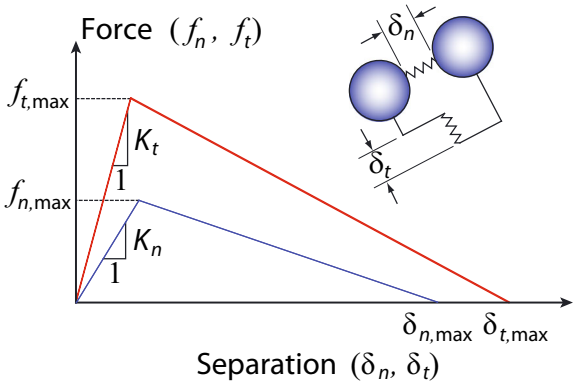

Fig. 6 Cohesive contact model between adjacent balls used in the heterogeneous DEM models. The traction-separation relationships in the normal (*n*) and tangential (*t*) directions are based on a linear softening cohesive contact model

asphalt concrete generally behave as a viscoelastic material at low temperatures as shown by the creep compliance test results in Fig. 3. Therefore, it is necessary to consider the time-dependent response of the mastic in heterogeneous fracture simulations. The current study can provide an initial indication if there is a need for a viscoelastic cohesive contact in heterogeneous DEM simulations at this particular temperature and set of loading rates. The use of viscoelastic assumptions might also be helpful with higher testing temperatures and slower testing rates. The user-defined model uses the interconverted mastic relaxation modulus results from the Burger's model fit to identify stiffness and viscosity properties. The viscoelastic response of the model was verified using a step stress relaxation test and reacts in a viscoelastic fashion prior to reaching the peak force of the cohesive bond between particles (f_{max}). The viscoelastic contact model only differs from the elastic cohesive contact model in the initial loading portion prior to reaching the peak force. After reaching the peak force, the viscoelastic model follows a linear softening model to zero cohesive force at the maximum cohesive bond displacement (δ_{max}) in the same fashion as the elastic bilinear cohesive model. Results obtained using both bilinear contacts and the user-defined viscoelastic contacts are discussed later in the "Results"section.

The primary advantage of DEM applications to asphalt mixture fracture is their ability to consider heterogeneous microstructures in a relatively simple way. Figure 7 illustrates the procedure to obtain a heterogeneous DEM geometry based on an asphalt test specimen. First, the test specimen is imaged using a 21.1 megapixel Canon EOS 5D Mark II camera with an EF 180 mm f/3.5 L Macro Lens. This image is then converted into a binary image using a Matlab image processing tool. Next, aggregate particles larger than 2.36 mm are identified using the Matlab blob analysis. Aggregate pixels are re-assigned a value of 1 and remaining pixels within the test geometry are re-assigned the value of 0 to correspond to the mastic. This leads to a binary image as depicted on the left side of Fig. 7. Then, DEM particles (balls) are superimposed to the image. These particles are placed following a hexahedral packing structure as recommended by Kim et al. [8]. A radius of 0.3 mm is chosen to model aggregate particles and reduce computational time. After the DEM particles are superimposed to the binary image, two DEM particle groups (called aggregate and mastic groups) are identified. If the centroid of a ball falls inside a region with a pixel value of 1, it is assigned to the aggregate group, otherwise it is assigned to the mastic group. In the case that aggregate particles are adjacent to mastic particles, an interface group is assigned. This leads to the DEM heterogeneous microstructure shown on the right side of Fig. 7.

After the DEM heterogeneous geometry has been created, particle bond properties are assigned to each DEM particle group. These bond properties include stiffness, strength, and fracture energy. Stiffness and strength properties are provided in both the normal and shear directions to account for separation and shear. The contact stiffness is determined using equation (4), the Poisson's Ratio is taken as $\nu = 0.33$, and the elastic modulus E is equal to the initial mastic relaxation modulus found using the IDT test. However, when the user-defined viscoelastic contact model is used, the contact stiffness between particles in the mastic group is obtained from the mastic relaxation modulus results. The maximum contact force and maximum contact displacement for particles in the aggregate group are approximately equal to those used in Kim et al. [6] because the same type of aggregate was used in this study. During the initial calibration phase of the following section, the peak force of the coarse aggregate particle bonds was increased by 27.9 N. This was done to account for global peak force differences between the experiment and the DEM results, which were obtained using the initial set of fracture parameters (before optimization of fracture parameters is performed). Finally, the maximum contact force and fracture energy for particles in the mastic and interface group are obtained through the optimization process, as explained in the next section. Fracture of asphalt concrete at −12 °C can lead to cracking in both the mastic and coarse aggregates. However, the majority of fracture occurred in the asphalt mastic and at the interface of the coarse aggregate. Consequently, the focus of the study was completed on mastic property optimization.[2] In addition, although local mixed-mode fracture occurs in heterogeneous DEM simulations, only Mode I opening properties are optimized in the current study – this approach is used because HMA is generally weak in tension.[3]

The interface (between aggregate and mastic) properties follows the recommendations by Kim et al. [8], namely the

[2] Future research could focus on aggregate fracture property identification using fracture tests in conjunction with DIC measurements.

[3] Additional future research could investigate the optimization of mixed-mode fracture properties.

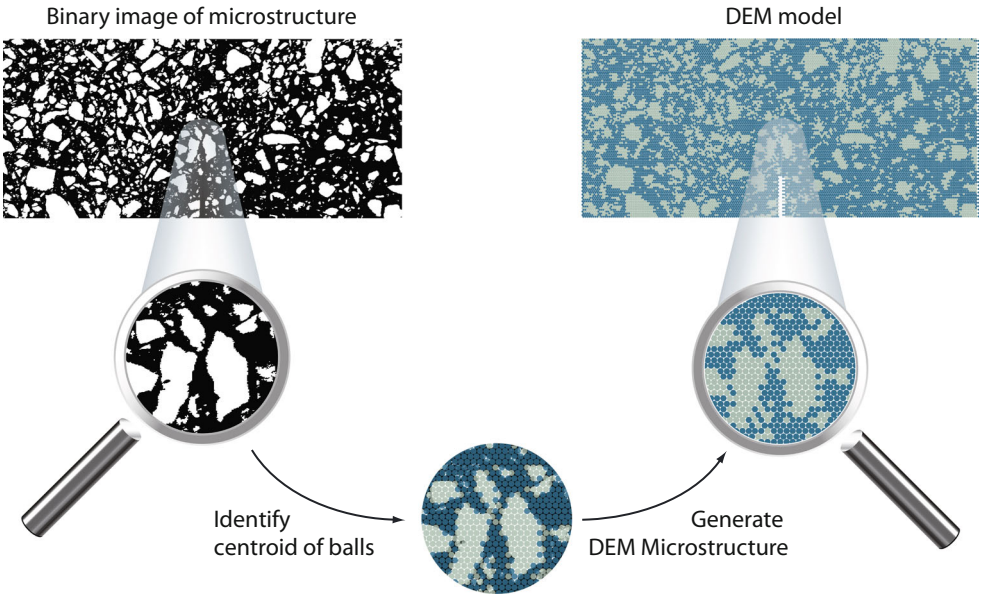

Fig. 7 Procedure used to develop the heterogeneous DEM model geometries. A binary image of the microstructure (*left*) for each geometry is used to locate the centroid of the balls such that the DEM models (*right*) resemble the microstructure of the specimens

maximum contact strength is about 90–100% of that of the mastic, and the maximum contact opening displacement is about 30% of that of the mastic. We chose these interface contact properties because they have shown to be suitable for DEM simulations of heterogeneous asphalt mixtures [4]. Research completed in the current study confirmed that the assumed ratios by Kim et al. [8] were comparable with experimental measurements of interface peak force and maximum displacement by Hakimzadeh [31]. Therefore, these ratios are used to obtain the fracture energy and cohesive strength for particles in the interface group. This leaves us with fracture energy and contact strength in the mastic group as the variables to be obtained through the optimization process.

Hybrid DIC-DEM Optimization Technique

Here we present a nonlinear optimization method to find the cohesive fracture properties of SE(B) and DC(T) test specimens. The method consists of minimizing the difference between the displacement fields from DIC and heterogeneous DEM simulations. To quantify this difference, the DEM and DIC displacement field vectors are measured at a number of grid points, n_n, near the notch tip. For each grid point, the displacement field vector is measured for n_p different values of CMOD. Then, the square of the Euclidean norm of the difference between the DEM and DIC displacement field vectors, obtained for all the grid points, is summed. This leads to the following measure as shown in equation (5):

$$\Phi(\boldsymbol{\lambda}) = \sum_{j=1}^{n_p}\sum_{i=1}^{n_n}\left\|\mathbf{u}_{DIC}^{(i,j)} - \mathbf{u}_{DEM}^{(i,j)}(\boldsymbol{\lambda})\right\|_2^2 \tag{5}$$

where $\Phi(\boldsymbol{\lambda})$ is the difference function or objective function; $\boldsymbol{\lambda}$ is the set of fracture parameters (e.g., cohesive strength and maximum crack opening) used for each one of the DEM simulations; $\mathbf{u}_{DIC}^{(i,j)}$ and $\mathbf{u}_{DEM}^{(i,j)}$ are the displacement field vectors at the grid point i for the jth value of CMOD.

A total of sixteen grid points near the notch tip (i.e., $n_n = 16$) are selected to measure the displacement fields for both DC(T) and SE(B) geometries. The grid points are located at 4.5 and 9 mm on each side of the notch tip, and spaced 1.5 mm in the direction parallel to the notch. In contrast to Shen and Paulino [14, 15], we selected a total of $n_p = 10$ CMOD values. The first value of CMOD is chosen at the point of peak load on the load-CMOD curve, and the following nine points are chosen at CMOD increments of 0.05 mm. For the DC(T) models, the peak load corresponds to a value of CMOD ≈ 0.10 mm, and for the SE(B) models it corresponds to CMOD ≈ 0.05 mm.

The evaluation of $\Phi(\boldsymbol{\lambda})$ is expensive because performing DEM simulations requires significant CPU time. The selection of an appropriate optimization algorithm is important to obtain the set of fracture parameters $\boldsymbol{\lambda}$ that minimizes $\Phi(\boldsymbol{\lambda})$ with a relatively small computational cost. In a typical optimization problem, efficient Newton-like methods are suitable choices to minimize the objective function. Although efficient, these methods require at least evaluating the gradient of the objective function, but this is computationally expensive for our problem. Therefore, alternative optimization methods, such as the derivative-free Nelder-Mead optimization method, are explored [14, 15]. The Nelder-Mead method, although simple and effective for the problems studied in [14, 15], is not suitable in our study. This is because, in general, the Nelder-Mead method requires hundreds of iterations [i.e., hundreds of function evaluations as the one given in equation

(5)] to achieve a desired level of accuracy, and as previously discussed, this is computationally expensive.

To minimize the required number of function evaluations, additional alternatives are considered. For instance, McDonald et al. [32] presented an optimization technique using radial basis functions to obtain a continuous representation of the objective function based on its values at a scattered set of points. This continuous function, called the response surface model, interpolates the objective function values at a given set of parameter values, reducing the required computation time dramatically.

Using the method by McDonald et al. [32] can lead to many different solutions, because different response surface models can be obtained for the same set of data points and the same choice of radial basis function. To circumvent this issue, the authors propose an alternative optimization method that uses multivariate Lagrange interpolation to approximate the objective function $\Phi(\boldsymbol{\lambda})$. The idea consists of obtaining a continuous multinomial $P(\boldsymbol{\lambda})$ that interpolates the values of $\Phi(\boldsymbol{\lambda})$ at a predefined set of fracture parameters $\boldsymbol{\lambda}^{(k)}$, $k = 1,\ldots, n$. Because multivariate Lagrange interpolation is used, the multinomial $P(\boldsymbol{\lambda})$ is uniquely defined. By construction, the interpolating multinomial $P(\boldsymbol{\lambda})$ is a C^{∞} function. Once this function is obtained, approximate values of the objective function and its gradient can be obtained in the entire fracture parameter space. Thus, efficient Newton-like methods can be utilized to perform the optimization process on $P(\boldsymbol{\lambda})$ avoiding evaluation of $\Phi(\boldsymbol{\lambda})$.

The space of fracture parameters, $\boldsymbol{\lambda}$, is defined next. As explained in the previous section, only the contact strength and fracture energy for particles in the mastic group are obtained through the optimization process. As shown in Fig. 6, we use a linear cohesive contact model (CCM). Hence, the fracture energy between adjacent particles is defined in terms of the contact strength ($f_{n,\max}$ and $f_{t,\max}$) and the maximum separation between particles ($\delta_{n,\max}$ and $\delta_{t,\max}$). Therefore, we can use these as the independent variables defining the CCM. Moreover, we assume that the fracture properties for the normal and tangential cohesive contacts are the same[4] (i.e., $f_{n,\max} = f_{t,\max} = f_{\max}$ and $\delta_{n,\max} = \delta_{t,\max} = \delta_{\max}$). Therefore, only two independent parameters, $f_{\max}$ and $\delta_{\max}$, are required to define the space of fracture parameters, $\boldsymbol{\lambda}$.

To obtain $P(\boldsymbol{\lambda})$, the difference function $\Phi(\boldsymbol{\lambda})$, given by equation (5), is evaluated at a given set of fracture parameters. This set of fracture parameters is determined by varying $f_{\max}$ between $f^1_{\max}$ and $f^n_{\max}$, and $\delta_{\max}$ between $\delta^1_{\max}$ and $\delta^n_{\max}$. This leads to a grid of fracture parameters, as shown in Fig. 8. The center of the parameter grid is chosen based on a pair of calibrated fracture parameters $\left(f^{cal}_{\max}, \delta^{cal}_{\max}\right)$, obtained in accordance to the study by Kim [4]. Kim's study suggested that

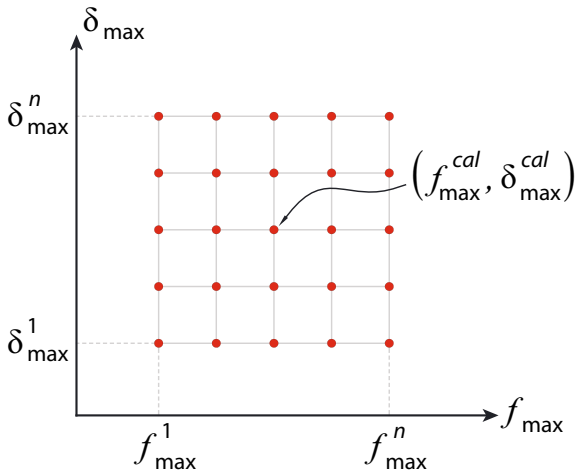

Fig. 8 Grid of fracture parameters used to obtain the interpolating multinomial P(λ)

the cohesive strength and fracture energy to be used with the DEM models should be approximately 74% of the experimentally measured values. Based on the results in [4], we expect that the optimum set of fracture parameters $\left(f^{opt}_{\max}, \delta^{opt}_{\max}\right)$ that leads to an accurate prediction of local fracture behavior of the asphalt specimens is in the vicinity of $\left(f^{cal}_{\max}, \delta^{cal}_{\max}\right)$. For the asphalt mixture tested in this study, the calibrated fracture parameters obtained for the SE(B) geometry are $\left(f^{cal}_{\max}, \delta^{cal}_{\max}\right) = \left(71\,\mathrm{N}, 1.14 \times 10^{-4}\mathrm{m}\right)$. After several attempts, we found that a grid of fracture parameters with $f_{\max} = [0.8, 0.9, 1.0, 1.1, 1.2] f^{cal}_{\max}$, and $\delta_{\max} = [0.8, 0.9, 1.0, 1.1, 1.2]\delta^{cal}_{\max}$ provided enough breadth to find the optimum of the objective function $\Phi(\boldsymbol{\lambda})$ for the SE(B) geometry. For the DC(T) geometry, an adequate grid of fracture parameters was found to be $f_{\max} = [0.8, 0.9, 1.0, 1.1, 1.2, 1.3] f^{cal}_{\max}$, and $\delta_{\max} = [0.8, 0.9, 1.0, 1.1, 1.2, 1.3]\delta^{cal}_{\max}$. The use of 10% intervals for both $f_{\max}$ and $\delta_{\max}$ helps to reduce the number of simulations needed to find the optimal solution. If a more detailed level of accuracy is desired, a finer grid of fracture parameters can be used. However, this would require performing more DEM fracture simulations.

Then, the inverse optimization problem using the Lagrange interpolating multinomial $P(\boldsymbol{\lambda})$ is formulated as shown below in equation (6):

$$\begin{aligned} &\min_{(f_{\max},\delta_{\max})} P(f_{\max},\delta_{\max}) = \sum_{p=1}^{n}\sum_{q=1}^{n} \Phi_{pq}\ell_p(f_{\max})\ell_q(\delta_{\max}), \\ &\Phi_{pq} = \sum_{j=1}^{n_p}\sum_{i=1}^{n_n}\left\|\mathbf{u}^{(i,j)}_{DIC} - \mathbf{u}^{(i,j)}_{DEM}\left(f^p_{\max},\delta^q_{\max}\right)\right\|_2^2, \\ &\ell_p(f_{\max}) = \prod_{\substack{m=1 \\ m\neq p}}^{n} \frac{f_{\max}-f^m_{\max}}{f^p_{\max}-f^m_{\max}}, \ell_q(\delta_{\max}) = \prod_{\substack{m=1 \\ m\neq q}}^{n} \frac{\delta_{\max}-\delta^m_{\max}}{\delta^q_{\max}-\delta^m_{\max}} \end{aligned} \tag{6}$$

where Φ_{pq} is the difference function computed from equation (5); $\ell_p(f_{\max})$ are 1-D Lagrange polynomials for the parameter $f_{\max}$; and $\ell_q(\delta_{\max})$ are the 1-D Lagrange polynomials for the parameter $\delta_{\max}$.

[4] This is questionable, however, in the absence of experimental information, this assumption was used.

The inverse problem shown in the optimization statement (6) uses the continuous function $P(\boldsymbol{\lambda})$ which interpolates $\Phi(\boldsymbol{\lambda})$ at each point $\left(f^i_{\max}, \delta^j_{\max}\right)$, for $i, j = 1,\ldots, n$ in the grid of fracture parameters. Thus, efficient Newton-like methods can be utilized to perform the optimization process on $P(\boldsymbol{\lambda})$ instead of $\Phi(\boldsymbol{\lambda})$. This step saves CPU time due to the reduced number of simulations required in the optimization.

Results

The first subsection below shows the experimental load-CMOD curves as well as the DIC results for both SE(B) and DC(T) geometries. Then, the next two subsections provide the optimization results for both geometries, following the procedure discussed in the previous Section.

Experimental Results

The load-CMOD curves obtained from both the DC(T) and SE(B) experiments are shown in Fig. 9. The optimal DEM simulation results are also shown in Fig. 9, however, they will be discussed subsequently. The SE(B) test yields a CMOD fracture energy that is 156.4 J/m^2 higher than the DC(T) test, and a peak load 1.13 kN higher than the DC(T) test. Similar results were found by Wagoner [3] when comparing SE(B) to DC(T) test results for a common asphalt mixture. Greater load capacity and fracture resistance is found in the SE(B) geometry because of the amount of energy consumed in bending. As stated by Wagoner [3], the DC(T) test is more prevalently used in the asphalt industry than the SE(B) due to the circular shape of asphalt core samples and their direct tensile load application.

The DIC full displacement fields (which include rigid body motions) for the DC(T) and SE(B) geometries are shown in Figs. 10 and 11, respectively. We observe that the rigid body motion associated with the DC(T) test is more pronounced than in the SE(B) test. This is due to the difference in the setup of the two experiments. For instance, in the DC(T) test, the specimen is loaded with pins inserted in the two pin holes. The bottom pin is held fixed, while the top pin moves vertically during the test. This allows for vertical translations and rotations, as observed in Fig. 10. The SE(B) test, however, consists of a beam with a center notch, which is loaded in a three-point bending test configuration. From a practical viewpoint, due to the more symmetric nature of this test, the rigid body motion is smaller than the one in the DC(T) test. Further observations show that the DIC displacement fields for the DC(T) geometry display greater crack tortuosity, which may be a function of the direct tensile loading method in the DC(T) test.

Numerical SE(B) Optimization Results

The optimization results for the SE(B) models are shown in Fig. 12. The elastic model results are shown in Fig. 12a, and the viscoelastic ones in Fig. 12b. The red dots correspond to the values of Φ_{pq} (see second expression in the optimization statement (6)) computed at the grid of fracture parameters described in the "Hybrid DIC-DEM Optimization Technique" section. The values of Φ_{pq} were used to construct the Lagrange interpolating multinomial for the optimization process. This multinomial corresponds to the surface interpolating the red dots in Fig. 12. Then, the Newton-Raphson method was used to determine the corresponding set of optimum fracture parameters $\left(f^{opt}_{\max}, \delta^{opt}_{\max}\right)$. For the elastic models, we obtained $\left(f^{opt}_{\max}, \delta^{opt}_{\max}\right) = \left(71\,\mathrm{N}, 1.2 \times 10^{-4}\,\mathrm{m}\right)$; and for the viscoelastic models, we obtained $\left(f^{opt}_{\max}, \delta^{opt}_{\max}\right) = \left(62\,\mathrm{N}, 1.1 \times 10^{-4}\,\mathrm{m}\right)$. A comparison can be drawn between those results. The

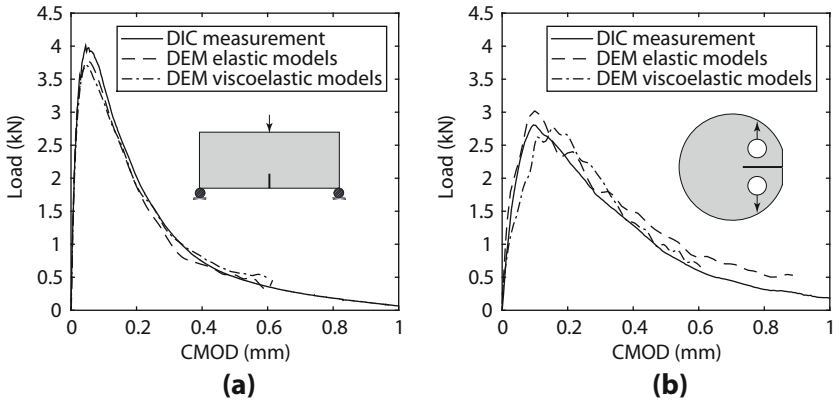

Fig. 9 Numerical and experimental Load-CMOD curves for: (**a**) SE(B) test; and (**b**) DC(T) test. The numerical results shown here correspond to those obtained from the set of fracture parameters associated to the minimization statement (6)

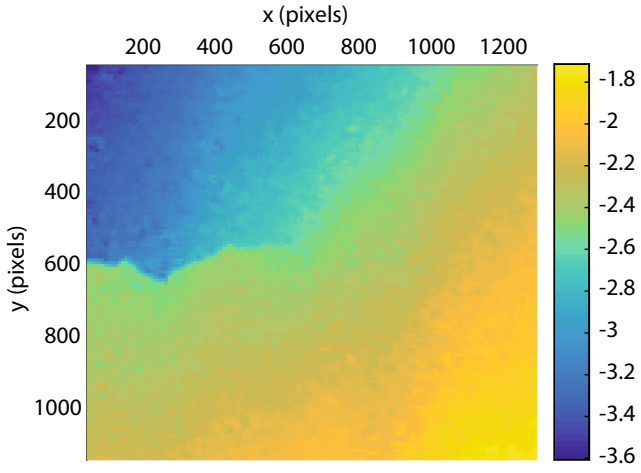

Fig. 10 DIC displacement field in the vertical direction (u_y) for a DC(T) test

difference in the optimization results between Fig. 12a and 12b demonstrates how viscoelastic creep affects DEM-measured displacements. As can be inferred from Fig. 12b, when the contact strength, $f_{\max}$, is larger, more viscoelastic deformations are allowed before softening occurs. Therefore, the difference between the DEM and DIC displacement measurements increases. To compensate for creep effects, the optimized fracture parameters in the viscoelastic models are slightly smaller than the ones in the elastic models. Finally, the experimental Load-CMOD is compared with the simulation results obtained with the optimized DEM fracture parameters, as shown in Fig. 9a. We observe that the optimal simulation results for both the elastic and viscoelastic simulation cases match the global Load-CMOD. Thus, this coupled DEM-DIC approach is applicable to Mode I simulations of an asphalt concrete beam geometry.

Numerical DC(T) Optimization Results

The optimization results for the DC(T) models are shown in Fig. 13. As stated previously, the values of Φ_{pq} in the optimization statement (6) were used to construct the Lagrange interpolating multinomial are represented by red dots. The green dots in Fig. 13 show the set of optimum fracture parameters obtained, which are $\left(f_{\max}^{opt}, \delta_{\max}^{opt}\right) = (85\ \text{N}, 1.3 \times 10^{-4}\ \text{m})$ and $\left(f_{\max}^{opt}, \delta_{\max}^{opt}\right) = (83\ \text{N}, 1.2 \times 10^{-4}\ \text{m})$ for the elastic and viscoelastic models, respectively. In regard to creep effects, similar observations to the SE(B) are found for the DC(T) models. That is, as the contact strength increases, the difference between DEM and DIC displacements increases. Thus, the optimal set of fracture parameters relative to the one from the elastic models shifts. As observed for the SE(B) test, the optimal DC(T) simulation results for both the elastic and viscoelastic models cases match the global Load-CMOD response shown in Fig. 9b. Consequently, this coupled DEM-DIC approach is applicable to Mode I simulations of an asphalt concrete DC(T) geometry as well.

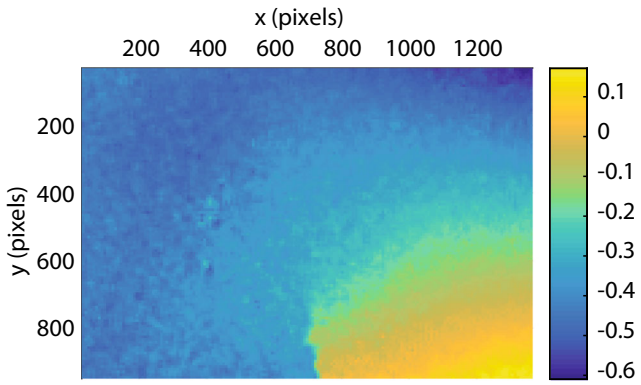

Fig. 11 DIC displacement field in the horizontal direction (u_x) for a SE(B) test

Comparing the results from both the SE(B) and DC(T) tests, we observe that the optimized contact strength for the SE(B) models is smaller than that one for the DC(T) models. This difference is mainly attributed to the fact that the SE(B) specimens are 25% thinner than the DC(T) specimens. This correlates with the known fact that asphalt concrete exhibits size-dependency, and specimen thickness affects material strength [3]. Additional differences in the optimization results are attributed to load application rates in both tests. For instance, the SE(B) test uses a loading rate that is smaller than the one used for the DC(T) test. The reduced loading rate in the SE(B) test allows for a greater amount of creep in the material, potentially affecting the optimization results.

Summary, Conclusions and Extensions

In this study, experimental DIC and numerical DEM displacement fields from two standard fracture tests are used to obtain the local fracture properties of asphalt concrete. Unlike previous studies, no predefined crack path is specified for the heterogeneous DEM simulations. A nonlinear optimization method is utilized to obtain the cohesive fracture properties of asphalt mixtures, which consists of computing the difference between DIC and DEM displacement fields for a predefined set of fracture parameters. Then, multivariate Lagrange interpolation is used to convert this discrete set of difference measurements into a continuous function, which is minimized using a Newton-like optimization algorithm. The DIC displacement fields are obtained via the Subset Splitting algorithm. For the DEM models, the predominantly mode-I fracture behavior is simulated using a linear softening cohesive contact model, where different fracture properties, including maximum tensile force and maximum crack opening, were varied within predefined values.

The proposed method is applied to two standard fracture test geometries: 1) an SE(B) under three-point bending

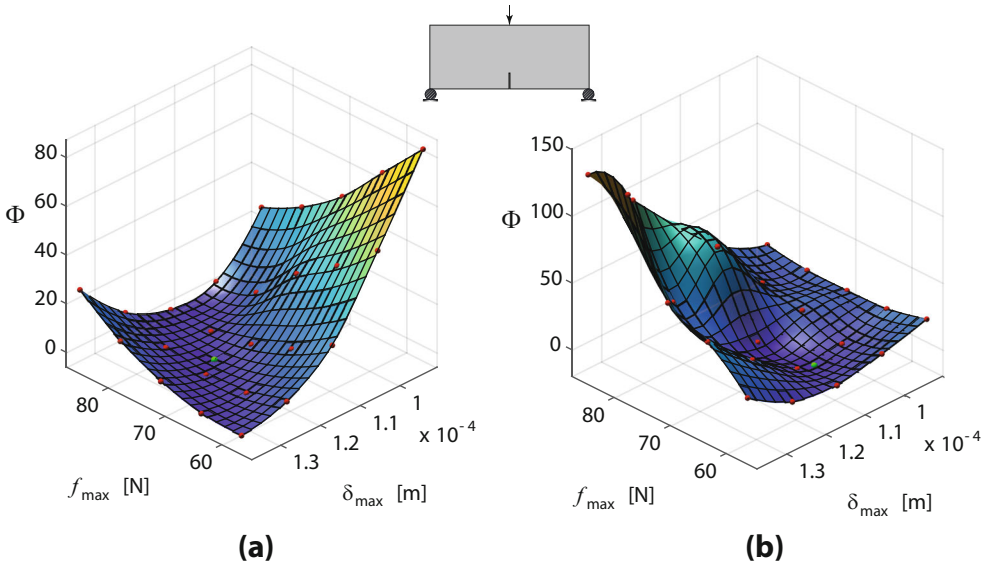

Fig. 12 Difference function '$\Phi(\lambda)$' evaluated at the grid of fracture parameters, and interpolating multinomial '$P(\lambda)$' for SE(B): (**a**) elastic models; and (**b**) viscoelastic models

geometry; and 2) a DC(T) geometry. The optimized set of fracture parameters from this nonlinear optimization method led to DEM results which are consistent with the experimental results for both SE(B) and DC(T) geometries. Thus, this method is a promising optimization approach when function evaluations are expensive; e.g., when simulating fracture in heterogeneous materials such as asphalt concrete. It can also be observed that:

- The difference between the optimal peak force for the SE(B) and DC(T) data sets was likely due to the 25% reduction in thickness found using the SE(B) geometry. If the viscoelastic DC(T) peak force was reduced by 25%, the optimal solutions would be approximately equal.
- The relative difference between the viscoelastic and elastic results was higher in the SE(B) geometry as compared to the DC(T). The largest differences were observed in the peak force, most likely due to the nature of the SE(B) geometry (bending/fracture), where the dissipative effects of the bulk viscoelasticity are more pronounced.

The next step in using this hybrid DIC-DEM approach will be to develop a library of optimum fracture properties for an array of asphalt mixtures. This library could be used in

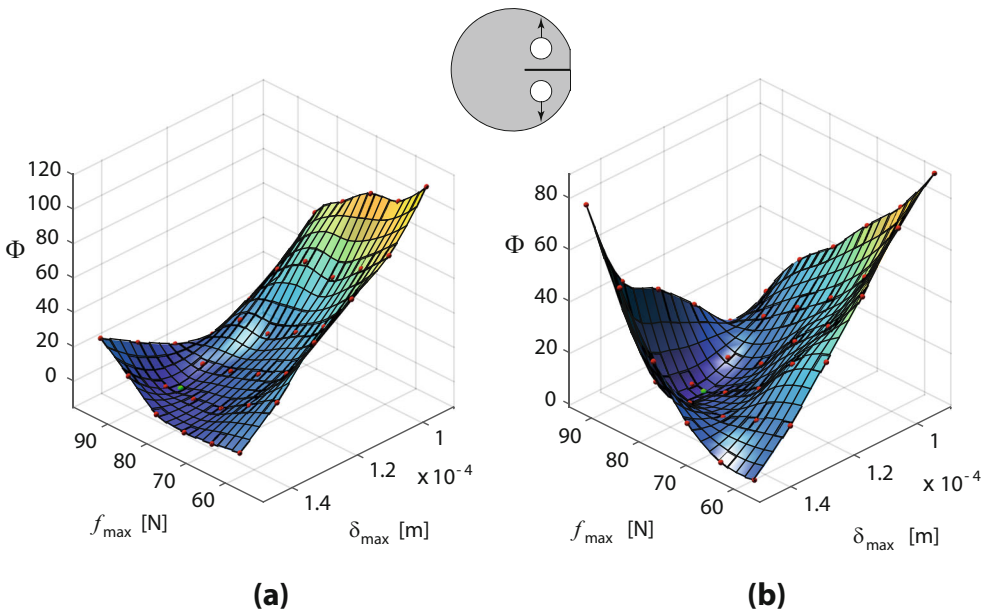

Fig. 13 Difference function '$\Phi(\lambda)$' evaluated at the grid of fracture parameters, and interpolating multinomial '$P(\lambda)$' for the DC(T): (**a**) elastic models; and (**b**) viscoelastic models

conjunction with 2D or 3D DEM simulations of pavement structures to simulate asphalt pavements undergoing thermal and vehicular loading at low temperatures. The simulation results could be used in academia and higher level mixture design firms to determine if an asphalt mixture has the potential to withstand a specified number of load applications.

Acknowledgements This material is based upon work supported by the National Science Foundation under Grant No. 1031218. Any opinions, findings, and conclusions or recommendations expressed in this material are those of the author(s) and do not necessarily reflect the views of the National Science Foundation.

References

1. Islam S, Buttlar WG (2012) Effect of pavement roughness on user costs. Journal of the Transportation Research Record 2285:47–55
2. Wagoner MP, Buttlar WG, Paulino GP (2005) Development of a single-edge notched beam test for asphalt concrete mixtures. J Testing and Evaluation 33(6):1–9
3. Wagoner MP (2006) Fracture tests for bituminous-aggregate mixtures: laboratory and field investigations. University of Illinois at Urbana-Champaign, PhD Dissertation
4. Kim H (2007) Investigation of toughening mechanisms in the fracture of asphalt concrete using the clustered discrete element method. Ph.D. Dissertation, University of Illinois at Urbana-Champaign
5. D'Addetta GA (2004) Discrete models for cohesive frictional materials. Rep. No. 42, Institute of Structural Mechanics, Univ. of Stuttgart, Stuttgart, Germany
6. Kim H, Wagoner MP, Buttlar WG (2009) Micromechanical fracture modeling of asphalt concrete using a single-edge notched beam test. Mater Struct 42(5):677–689
7. Kim H, Wagoner MP, Buttlar WG (2009) Numerical fracture analysis on the specimen size dependency of asphalt concrete using a cohesive softening model. Constr Build Mater 23:2112–2120
8. Kim H, Wagoner MP, Buttlar WG (2008) Simulation of fracture behavior in asphalt concrete using a heterogeneous cohesive zone discrete element model. J Mater Civ Eng 20:552–563
9. Kim H, Buttlar WG (2005) Micromechanical fracture modeling of asphalt mixture using the discrete element method. Proc., GeoFrontier 2005, ASCE, Reston, Va
10. Aragão FTS, Kim Y (2012) Mode I fracture characterization of bituminous paving mixtures at intermediate service temperatures. Exp Mech 52(9):1423–1434
11. Kim Y, Aragão FTS (2013) Microstructure modeling of rate-dependent fracture behavior in bituminous paving mixtures. Finite Elem Analysis Des 63:23–32
12. Im S, Ban H, Kim Y (2014) Characterization of mode-I and mode-II fracture properties of fine aggregate matrix using a semicircular specimen geometry. Constr Build Mater 52:413–421
13. Pop O, Meite M, Dubois F, Absi J (2011) Identification algorithm for fracture parameters by combining DIC and FEM approaches. Int J Fract 170:101–114
14. Shen B, Paulino GH (2011) Direct extraction of cohesive fracture properties from digital image correlation: a hybrid inverse technique. Exp Mech 51:143–163
15. Shen B, Paulino GH (2011) Identification of cohesive zone model and elastic parameters of fiber-reinforced cementitious composites using digital image correlation and a hybrid inverse technique. Cement Concr Compos 33:572–585
16. Cundall PA, Strack ODL (1979) A discrete numerical model for granular assemblies. Journal of Geotechnique 29:47–65
17. AASHTO M323 (2004) Standard specification for superpave volumetric mix design. AASHTO Standard Specifications for Transportation Materials and Methods of Sampling and Testing. Washington, D.C.
18. ASTM D7313-13 (2013) Standard test method for determining fracture energy of asphalt-aggregate mixtures using the disk-shaped compact tension geometry. American Society for Testing and Materials International. West Conshohocken, PA
19. AASHTO T322 (2007) Standard method of test for determining the creep compliance and strength of hot-nix asphalt (HMA) using the indirect tensile test device. AASHTO Standard Specifications for Transportation Materials and Methods of Sampling and Testing. Washington, D.C.
20. Park S, Kim Y (1999) Interconversion between relaxation modulus and creep compliance for viscoelastic solids. J Mater Civ Eng 11(1): 76–82
21. Swaminathan B, Lambros J, Sehitoglu H (2013) Digital image correlation study of mechanical response of nickel superalloy Hastelloy X under thermal and mechanical cycling: Uniaxial and biaxial stress states. J Strain Analysis Special Issue 49(4):233–243
22. Abanto-Bueno J, Lambros J (2002) Investigation of crack growth in functionally graded materials using digital image correlation. J Engineering Fracture Mechanics 69:1695–1711
23. Meite M, Dubois F, Pop O, Absi J (2013) Mixed mode fracture properties characterization for wood by digital images correlation and finite element method coupling. Journal of Engineering Fracture Mechanics 105:86–100
24. Carroll JD, Abuzaid W, Lambros J, Sehitoglu H (2013) High resolution digital image correlation measurements of strain accumulation in fatigue crack growth. Int J Fatigue 57:140–150
25. Poissant J, Barthelat F (2010) A novel subset splitting procedure for digital image correlation on discontinuous displacement fields. Exp Mech 50(3):353–364
26. Hill B, Buttlar WG (2016) Evaluation of polymer modification in asphalt mixtures through digital image correlation and performance space diagrams. J Construction and Building Materials 122:667–673
27. You Z, Buttlar WG (2004) Discrete element modeling to predict the modulus of asphalt concrete mixtures. J Mater Civil Eng ASCE 16(2):140–146
28. Labuz JF, Cattaneo S, Chen L-H (2001) Acoustic emission at failure in quasi-brittle materials. Constr Build Mater 15:225–233
29. Li X, Marasteanu MO (2006) Investigation of low temperature cracking in asphalt mixtures by acoustic emission. Road Materials and Pavement Design 7(4):491–512
30. Li X, Marasteanu M, Iverson N, Labuz JF (2006) Observation of crack propagation in asphalt mixtures with acoustic emission. Transp Res Rec 1970:171–177
31 Hakimzadeh S (2015) Evaluation of bond between pavement layers: fracture mechanics approach. Ph.D. Dissertation, University of Illinois at Urbana-Champaign
32 McDonald DB, Grantham WJ, Tabor WL, Murphy MJ (2007) Global and local optimization using radial basis function response surface models. Appl Math Model 31:2095–2110